Inviscid Analysis of Two-Dimensional Airfoils in Unsteady Motion Using Conformal Mapping

D. H. Choi*
Korea Advanced Institute of Science and Technology, Seoul, Korea
and
L. Landweber†
University of Iowa, Iowa City, Iowa

Using a conformal mapping technique, a procedure for calculating the irrotational flow about a two-dimensional airfoil of arbitrary shape in unsteady motion is developed. The two-dimensional form with a sharp trailing edge is transformed into a unit circle by two successive transformations. The latter of the two is a modified version of the Gershgorin integral equation, which yields solutions much more accurate than those obtained with panel methods. The change in circulation around the airfoil due to unsteadiness is modeled by discrete vortices that are shed from the trailing edge and allowed to move freely with the local stream. The strength of these vortices is determined by the Kutta condition that, at each time step, the velocity be zero at the trailing edge in the circle plane. The procedure is efficient since the integral equation is solved only once. Numerical examples are presented for a sinusoidal heaving motion and for an impulsively started airfoil.

Introduction

INVISCID analysis of two-dimensional airfoils in unsteady motion has usually been treated by various panel methods based on surface singularity distributions.[1-4] For such methods, difficulty may arise as the trailing-edge angle becomes smaller since the discretized equations become nearly dependent and, consequently, the accuracy suffers in this region. Detailed discussions may be found in Refs. 3 and 5. This inaccuracy may be aggravated further if the flow is unsteady, as the change in circulation cannot be accurately determined. This is so because any form of the Kutta condition is related to conditions at the panels adjacent to the trailing edge. It also requires that the integral equation be solved at successive time steps. This may become rather time consuming when a very small time step and/or a large number of panels are used.

Methods based on conformal mapping have also been in wide use, but mostly for steady flows (see, e.g., Refs. 6 and 7). Poling et al.[8] recently used a conformal-mapping approach for the vortex-blade interaction study; however, the transformation was only approximate since they used an equivalent Joukowski airfoil in place of the NACA 0012 airfoil.

In the present paper, a method based on conformal mapping is presented. In this approach, since the potential is given analytically in the circle plane, the Kutta condition can be treated in an analytic manner. This ensures an accurate prediction of the flow development. Furthermore, the procedure is very efficient as the integral equation is solved only once when the body is transformed. The aforementioned shortcomings of the panel method can therefore be avoided.

Conformal Transformations

An airfoil with a sharp trailing edge is transformed into a unit circle by two successive transformations. The first, the Kármán-Trefftz transformation

$$\frac{z-\epsilon}{z-l}=\left(\frac{\zeta+1}{\zeta-1}\right)^p, \qquad p=2\left(1-\frac{\delta}{2\pi}\right) \tag{1}$$

maps the two-dimensional foil of length l with a trailing-edge angle δ into a smooth, nearly circular section in the ζ plane, as was done by Theodorsen[9] in the first practical conformal-mapping procedure. The origin O of the z plane is taken at the point of maximum curvature at the leading end of the foil. The nodal point at $(\epsilon,0)$ is then taken at half the distance from the origin O to the center of curvature of the section at O.

In terms of the bipolar coordinate systems (see Fig. 1) in the z and ζ planes, we obtain from Eq. (1),

$$\Lambda=\lambda^p, \qquad \Omega=p\omega \tag{2}$$

where $\Lambda=R_2/R_1$, $\lambda=r_2/r_1$, $\Omega=\psi_2-\psi_1$, and $\omega=\phi_2-\phi_1$. As is shown in Appendix A, the polar coordinates (r,ϕ) in the ζ plane relative to the origin at C are related to the bipolar coordinates (λ,ω) by the following relations:

$$r_1=(r^2+2r\cos\phi+1)^{1/2} \tag{3a}$$

$$r_2=(r^2-2r\cos\phi+1)^{1/2} \tag{3b}$$

$$\omega=\tan^{-1}\frac{2r\sin\phi}{r^2-1} \tag{4}$$

or conversely

$$r=\frac{1}{d}(\lambda^2+2\lambda\cos\omega+1)^{1/2}, \qquad \phi=\tan^{-1}\frac{2\lambda\sin\omega}{1-\lambda^2} \tag{5}$$

where

$$d=(\lambda^2-2\lambda\cos\omega+1)^{1/2}$$

Similar relations between the rectangular and bipolar coordinate systems may be written for points in the z plane. Let (X,Y) denote the nondimensional coordinates, with the origin at the midpoint E of NT, such that

$$x=\tfrac{1}{2}(l+\epsilon)+\tfrac{1}{2}(l-\epsilon)X, \qquad y=\tfrac{1}{2}(l-\epsilon)Y \tag{6}$$

Received July 10, 1989; revision received Jan. 3, 1990.

*Associate Professor, Department of Mechanical Engineering. Member AIAA.

†Emeritus Professor, Department of Mechanical Engineering, Institute of Hydraulic Research.

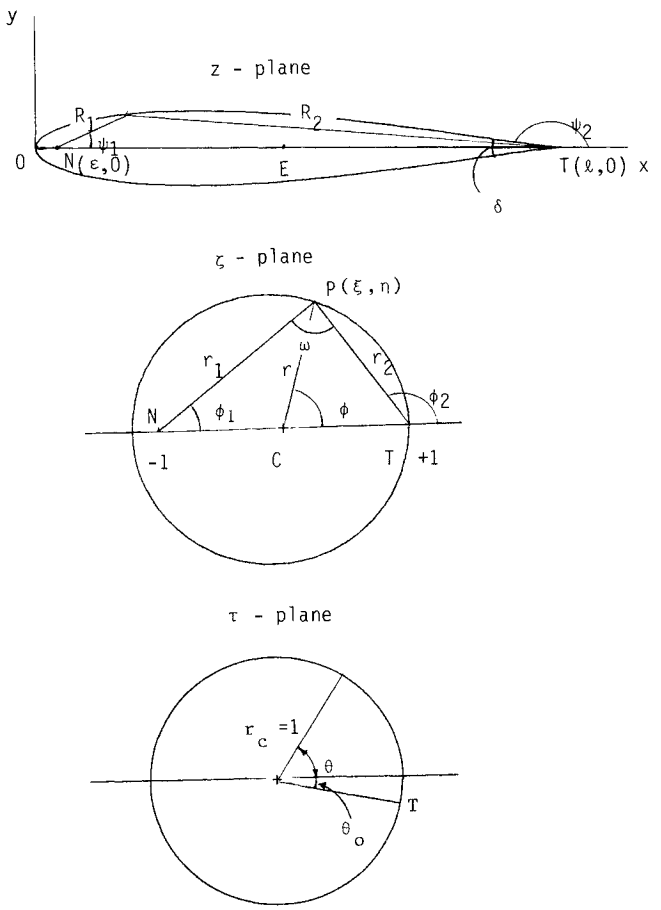

Fig. 1 Conformal transformations.

Then X and Y can be written as

$$X = \frac{1-\Lambda^2}{D^2}, \quad Y = \frac{2\Lambda}{D^2}\sin\Omega, \quad D = (\Lambda^2 - 2\Lambda\cos\Omega + 1)^{1/2} \tag{7}$$

The coordinates of corresponding points in the z and ζ planes can be found as follows. For a given point (x,y), λ and ω are given by Eq. (2). Then Eq. (5) gives r and ϕ. Conversely, for a given point (r,ϕ), λ is given by Eqs. (3) and ω by Eq. (4), Λ and Ω by Eq. (2) and (X,Y) and (x,y) by Eqs. (7) and (6).

The next step is to transform this nearly circular section in the ζ plane, $\zeta = r(\phi)e^{i\phi}$, into a unit circle in the τ plane, with $\tau = r_c e^{i\theta}$. Among the many available methods for performing this mapping, the Gershgorin integral equation,[10] which was included in a comparative numerical study of various conformal-mapping procedures by Birkhoff et al.,[6] was adopted. We believe that this method is more efficient and yields better accuracy than others that have been used for the mapping of airfoils. For the exterior mappings, this integral equation may be written as

$$\theta(\phi) = -\frac{1}{\pi}\int_{\phi}^{\phi+2\pi}\frac{\partial\chi(\phi,\phi')}{\partial\phi'}\theta'\,d\phi' + 2\gamma$$

$$\theta' = \theta(\phi'), \quad \gamma = \chi(\phi,\phi) \tag{8}$$

where χ, defined below, increases from $\gamma + n\pi$ to $\gamma + (n+1)\pi$ as ϕ' increases from $\phi + 2n\pi$ to $\phi + 2(n+1)\pi$ for any integer n. This defines χ as a continuous function. Here

$$\chi = \tan^{-1}\frac{r'\sin\phi' - r\sin\phi}{r'\cos\phi' - r\cos\phi}$$

$$\gamma = \tan^{-1}\frac{(dr/d\phi)\sin\phi + r\cos\phi}{(dr/d\phi)\cos\phi - r\sin\phi} \tag{9}$$

The kernel of the integral equation is then given by

$$\frac{\partial\chi}{\partial\phi'} = \frac{r'^2 - rr'\cos(\phi'-\phi) - r(dr'/d\phi')\sin(\phi'-\phi)}{r'^2 - 2rr'\cos(\phi'-\phi) + r^2}$$

$$\phi' \neq \phi \tag{10}$$

The angle γ in Eq. (8) is that of the tangent at a smooth point of the section in the limit as ϕ' approaches ϕ through values of $\phi' > \phi$. The kernel is regular, even at $\phi' = \phi$ where, as seen from Eq. (10), it is indeterminate, but, as shown in Ref. 10, its limiting value there is proportional to the curvature at that point.

Although Eq. (8) can be used directly to obtain a numerical solution, two modifications significantly reduce the computing effort and improve the accuracy of the numerical results, especially when the profile in the physical plane is not defined analytically. The modified equation is

$$\theta(\phi) = -\frac{1}{2\pi}\int_0^{2\pi}\frac{\partial\chi}{\partial\phi'}[\theta' - \theta - 2\chi + 2\gamma(\phi)]\,d\phi' + \gamma - \frac{\pi}{2} \tag{11}$$

Here, the term -2χ, first introduced in Ref. 6, makes the integrand cyclic, so that the integration limits may be changed to 0 and 2π with χ corresponding to $n = -1$ for $0 \le \phi' < \phi$ and to $n = 0$ for $\phi < \phi' \le 2\pi$. Hence, the most accurate quadrature formula, the trapezoidal rule, may be used (see Ref. 11). The terms $-\theta$ and $2\gamma(\phi)$, which are constant in the course of the integration, were first introduced in Ref. 10 to reduce the integrand to zero when $\phi' = \phi$, so that the calculation of the curvature could be avoided. An additional advantage is that this yields a form of the equation that is valid at corner points, although, practically, it is preferable to eliminate the corners, otherwise, many more terms of the Fourier expansion would be needed. One can readily verify that Eq. (11) is equivalent to Eq. (8) by noting that $2\chi\,\partial\chi/\partial\phi'$ can be integrated exactly, and by also applying the property

$$\int_0^{2\pi}\frac{\partial\chi}{\partial\phi'}\,d\phi' = \pi \tag{12}$$

In order to use the most accurate quadrature formula in discretizing Eq. (11), the intervals $\Delta\phi'$ must be constant. Denoting ϕ by ϕ_i and ϕ' by ϕ_j, θ by θ_i, θ' by θ_j, etc., we obtain

$$\theta_i^{(n+1)} = \gamma_i - \frac{\pi}{2} - \frac{\Delta\phi}{2\pi}\sum_{j=1}^{M}\left(\frac{\partial\chi}{\partial\phi'}\right)_{ij}[\theta_j^{(n)} - \theta_i^{(n)} - 2\chi_{ij} + 2\gamma_i] \tag{13}$$

for M intervals. Values at $j = i$, at which the integrand is zero, are not required. The superscripts (n) and $(n+1)$ indicate that the set of M linear equations in the unknowns $\theta_1, \theta_2, \ldots, \theta_M$ are to be solved by iteration, beginning for a nearly circular section, with $\theta_i = \phi_i$ as the first approximation.

The mapping function between the ζ and τ planes may then be expressed as the Laurent series:

$$\zeta = A\tau + \frac{a_1}{\tau} + \frac{a_2}{\tau^2} + \ldots \tag{14}$$

where

$$A = \frac{1}{2\pi}\int_0^{2\pi} r(\phi)e^{i(\phi-\theta)}\frac{d\theta}{d\phi}\,d\phi \tag{15}$$

$$a_n = \frac{1}{2\pi}\int_0^{2\pi} r(\phi)e^{i(\phi+n\theta)}\frac{d\theta}{d\phi}\,d\phi, \qquad n = 1,2\ldots \tag{16}$$

Pressure Distribution on the Airfoil Surface

Steady Motion

The velocity potential W for a stream of velocity U at an angle of attack α in the τ plane is

$$W = U\left(\tau e^{-i\alpha} + \frac{e^{i\alpha}}{\tau}\right) + ik\ell n\tau \tag{17}$$

where k is proportional to the circulation about the cylinder. This gives the velocity distribution about the cylinder

$$|V| = 4U \cos\left(\frac{\theta+\theta_0}{2} - \alpha\right) \sin\frac{1}{2}(\theta-\theta_0) \tag{18}$$

which satisfies the Kutta condition that the velocity be zero at the trailing edge T, $\theta = \theta_0$, with $k = 2U \sin(\alpha - \theta_0)$.

The complex velocity in the z plane is given by

$$\frac{dW}{dz} = \frac{dW}{d\tau}\frac{d\tau}{d\zeta}\frac{d\zeta}{dz} \tag{19}$$

where $dW/d\tau$ is obtained from Eqs. (17) and (22) and the other two factors from the mapping functions. The velocity at infinity in the z plane U_∞ differs from the value U in the τ plane since, by Eqs. (14) and (15),

$$\left(\frac{d\zeta}{d\tau}\right)_\infty = \frac{1}{2\pi}\int_0^{2\pi} r(\phi)\cos(\phi-\theta)\frac{d\theta}{d\phi}\,d\phi \tag{20}$$

$$\left(\frac{dz}{d\zeta}\right)_\infty = \frac{l-\epsilon}{2p} \tag{21}$$

Hence, taking $U_\infty = 1$, one obtains for the velocity U in the τ plane,

$$U = \frac{l-\epsilon}{4\pi p}\int_0^{2\pi} r(\phi)\cos(\theta-\phi)\frac{d\theta}{d\phi}\,d\phi \tag{22}$$

Unsteady Motion

From the Bernoulli equation for unsteady flow, the pressure coefficient may be written in a moving coordinate system attached to the body as

$$C_p = \frac{P-P_\infty}{\frac{1}{2}\rho U_\infty^2} = -2\frac{\partial\Phi}{\partial t} + 2\boldsymbol{V}\cdot(\boldsymbol{V}_0 + \boldsymbol{\Psi}\times\boldsymbol{R}_r) - V^2 \tag{23}$$

where Φ is the velocity potential, t the time, $\boldsymbol{V}$ the absolute velocity of a fluid particle, $\boldsymbol{V}_0$ the absolute velocity of the origin of the moving frame, $\boldsymbol{\Psi}$ the angular velocity of the moving frame, and $\boldsymbol{R}_r$ the position vector relative to that frame. Here, all of these quantities have been made dimensionless in terms of the characteristic velocity and length, i.e., U_∞ and the airfoil chord c, respectively.

When $\boldsymbol{V}_0(t)$ and $\boldsymbol{\Psi}(t)$ are prescribed, the mapping of the airfoil section into the τ plane remains valid, but the solution for the complex potential W, given by Eqs. (17) and (18) for the steady case, must be modified, as is done in the next section. Then, at each time step, $dW/d\tau$ yields $\boldsymbol{V}_r$, the velocity relative to the moving frame, and the absolute velocity $\boldsymbol{V}$ is given by

$$\boldsymbol{V} = \boldsymbol{V}_r + \boldsymbol{V}_0 + \boldsymbol{\Psi}\times\boldsymbol{R}_r \tag{24}$$

The pressure distribution can then be obtained from Eq. (23).

Wake Simulation

As the airfoil undergoes unsteady motion, the circulation around the profile changes continuously. Since the total circulation in the flowfield must be conserved as stated by the Kelvin-Helmholtz theorem, the change in circulation around the airfoil is matched by the change in circulation in the wake of equal magnitude and opposite sign. This can be achieved by shedding a point vortex from the airfoil trailing edge T at each time step. The strength of the vortex is chosen to satisfy the Kutta condition at that instant. The vortices so shed are convected by the local stream.

The path of each particle of the vortex in the inertial coordinate system would be determined by integrating the absolute velocity [Eq. (24)] with respect to time. However, since the vortex positions relative to the profile are of primary interest in the subsequent analysis, only the particle motion relative to the airfoil will be considered. It is important to point out here that, as we switch over to the relative frame of reference, the implementation of the Kelvin-Helmholtz theorem requires a careful treatment. As is shown in Appendix B, the conserved quantity, in a noninertial frame of reference, is the sum of the relative circulation about the airfoil and $2S\Psi$, where S is the cross-sectional area of the airfoil.

When N point vortices have been shed, the complex potential W in the τ plane may be written in the form

$$W = W_s - i\sum_{n=1}^{N} k_n[\ln(\tau-\tau_n) - \ln(\tau - 1/\bar{\tau}_n)] \tag{25}$$

in which the last term is due to the image of the nth vortex in the circle. Here, W_s is the potential for the steady flow [Eq. (17)], k_n the strength of the nth point vortex, and τ_n its position. In order to obtain the velocity of this vortex in the z or τ planes, we must exclude its own contribution to the velocity at τ_n or at the corresponding point z_n in the z plane. In order to relate these velocities, following Milne-Thomson,[12] we put

$$W_{zn} = W + ik_n\ln(z-z_n), \qquad W_{\tau n} = W + ik_n\ln(\tau-\tau_n) \tag{26}$$

Then

$$W_{zn} = W_{\tau n} + ik_n\ln\frac{z-z_n}{\tau-\tau_n}$$

and, in the limit as $\tau\to\tau_n$, this becomes

$$W_{zn} = W_{\tau n} + ik_n\ln\left(\frac{dz}{d\zeta}\frac{d\zeta}{d\tau}\right)_{\tau_n} \tag{27}$$

Hence,

$$\frac{dW_{zn}}{dz}\frac{dz}{d\zeta}\frac{d\zeta}{d\tau} = \frac{dW_{\tau n}}{d\tau} + ik_n\frac{\frac{dz}{d\zeta}\frac{d^2\zeta}{d\tau^2} + \frac{d^2z}{d\zeta^2}\left(\frac{d\zeta}{d\tau}\right)^2}{\frac{dz}{d\zeta}\frac{d\zeta}{d\tau}}$$

or

$$\frac{dW_{zn}}{dz} = \frac{dW_{\tau n}/d\tau}{\frac{dz}{d\zeta}\frac{d\zeta}{d\tau}} + ik_n\frac{\frac{dz}{d\zeta}\frac{d^2\zeta}{d\tau^2} + \frac{d^2z}{d\zeta^2}\left(\frac{d\zeta}{d\tau}\right)^2}{\left(\frac{dz}{d\zeta}\frac{d\zeta}{d\tau}\right)^2} \tag{28}$$

The conjugate of Eq. (28) then gives the velocity of the nth point vortex in the z plane.

The displacement of a vortex in the z plane for the interval dt is

$$dz = \overline{\frac{dW_{zn}}{dz}}\cdot dt \tag{29}$$

where t is time and the overbar indicates the conjugate. Since $dz = (dz/d\zeta)(d\zeta/d\tau)\,d\tau$, the corresponding displacement in the τ plane $d\tau$ can be written as

$$d\tau = \frac{\overline{(dW_{zn})}/(dz)}{(dz/d\zeta)(d\zeta/d\tau)}\,dt \tag{30}$$

Then the new vortex position in the τ plane is given as $\tau + d\tau$.

At each time step, the existing vortices are convected using Eq. (30) and then a new vortex is shed. It is of critical importance how the position and the strength of this nascent vortex are determined. The procedure is thus explained in some de-

tail. As the nascent vortex represents the vortex sheet element that has been shed during the time interval Δt, it is logical to assume that it be placed at the center of this element. The center can be approximated by the position of the particle that left the trailing edge at time $\Delta t/2$ earlier. The integration is done in two steps and since Eq. (30) is indeterminate at the trailing edge, the first step is performed analytically as follows.

Equation (30) may be rewritten, for a fluid particle, as

$$d\tau = \frac{\overline{\frac{dW}{d\tau}}}{\left|\frac{dz}{d\zeta}\right|^2 \left|\frac{d\zeta}{d\tau}\right|^2} dt \tag{31}$$

or

$$dt = \frac{\left|\frac{dz}{d\zeta}\right|^2 \left|\frac{d\zeta}{d\tau}\right|^2}{\overline{\frac{dW}{d\tau}}} d\tau \tag{32}$$

We wish to obtain an asymptotic expression of Eq. (32) near the trailing edge. Integration of this over a short distance will then give the desired relation between τ and t. Very close to the stagnation point $\tau = e^{i\theta_0}$ the flow is in the radial direction and the contribution in that direction of the vortices may be neglected. The radial velocity component may then be expressed as

$$u_r \approx \left|\overline{\frac{dW}{d\tau}}\right| \approx 2U\cos(\alpha-\theta_0)\cdot h \tag{33}$$

where h is the distance measured along the radial line from the trailing edge in the τ plane.

Of the remaining two factors in Eq. (32), $d\zeta/d\tau$ can be evaluated numerically using Eq. (14), whereas the expression for $dz/d\zeta$ is obtained from Eq. (1) as

$$\frac{dz}{d\zeta} \approx \frac{p}{2^p}(l-\epsilon)(\zeta-1)^{p-1} \tag{34}$$

Substituting Eq. (14) for ζ in Eq. (34) with $\tau=(1+h)e^{i\theta_0}$ and expanding the resulting equation in terms of h, we obtain

$$\frac{dz}{d\zeta} \approx \frac{p}{2^p}(l-\epsilon)[(Ae^{i\theta_0} - a_1 e^{-i\theta_0} - a_2 e^{-2i\theta_0} - \ldots.)h]^{p-1} \tag{35}$$

After substituting Eqs. (33) and (35) in Eq. (32), a simple integration with respect to h yields

$$t = \frac{h^{2(p-1)}}{K} \tag{36}$$

or

$$h = (Kt)^{\frac{1}{2(p-1)}} \tag{37}$$

where

$$K = \frac{4U(p-1)\cos(\alpha-\theta_0)}{\left[\frac{p}{2^p}(l-\epsilon)\right]^2 |Ae^{i\theta_0} - a_1 e^{-i\theta_0} - 2a_2 e^{-2i\theta_0}\ldots|^{2(p-1)} \cdot \left|\frac{d\zeta}{d\tau}\right|^2}$$

Equation (37) is now used to get an intermediate point τ_I with a very small time increment Δt_I ($<\Delta t/2$). The position of the nascent vortex τ_{N+1} is then determined using Eq. (30) with $\tau=\tau_I$, $k_n=0$, $dt=(\Delta t/2)-\Delta t_I$ and, hence, $\tau_{N+1}=\tau_I+d\tau$.

Table 1 Comparison of the pressure distribution along the upper surface of a Kármán-Trefftz airfoil for $\alpha=9$ deg

x	Exact	Present
0.00000D+00	−0.26358D+01	−0.26520D+01
0.41406D−02	−0.41659D+01	−0.41492D+01
0.16605D−01	−0.35942D+01	−0.35997D+01
0.37100D−01	−0.28963D+01	−0.28957D+01
0.65117D−01	−0.23884D+01	−0.23886D+01
0.10006D+00	−0.20195D+01	−0.20195D+01
0.14124D+00	−0.17360D+01	−0.17360D+01
0.18791D+00	−0.15052D+01	−0.15052D+01
0.23924D+00	−0.13085D+01	−0.13085D+01
0.29439D+00	−0.11352D+01	−0.11353D+01
0.35247D+00	−0.97904D+00	−0.97905D+00
0.41256D+00	−0.83622D+00	−0.83623D+00
0.47376D+00	−0.70457D+00	−0.70458D+00
0.53519D+00	−0.58276D+00	−0.58277D+00
0.59595D+00	−0.46996D+00	−0.46997D+00
0.65520D+00	−0.36559D+00	−0.36560D+00
0.71212D+00	−0.26921D+00	−0.26921D+00
0.76591D+00	−0.18038D+00	−0.18039D+00
0.81580D+00	−0.98653D−01	−0.98658D−01
0.86108D+00	−0.23459D−01	−0.23461D−01
0.90105D+00	0.45934D−01	0.45930D−01
0.93506D+00	0.11059D+00	0.11058D+00
0.96252D+00	0.17224D+00	0.17222D+00
0.98285D+00	0.23442D+00	0.23446D+00
0.99553D+00	0.30758D+00	0.30753D+00

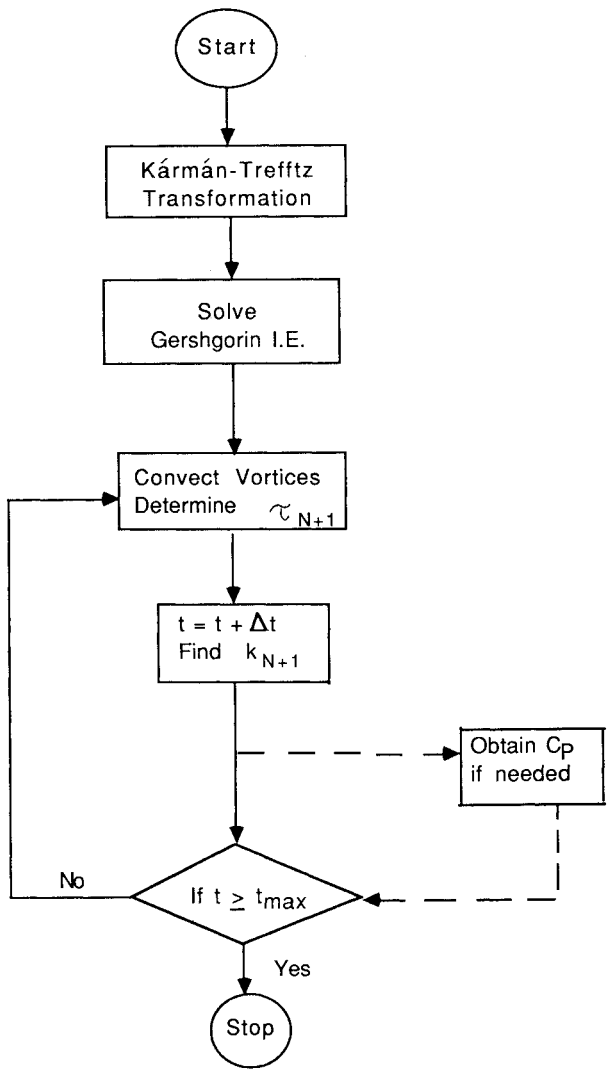

Fig. 2 Analysis procedure.

This treatment near the trailing edge is quite different from some of the earlier works[2,3,13] in which the streamline emanating from the trailing edge is assumed to be tangent to either the upper or lower surface depending on the sign of the circulation being shed. This hypothesis, which is referred to as the Giesing-Maskell model, breaks down as the rate of the circulation change becomes zero since it fails to recover the steady-state streamline, as was pointed out in Refs. 2 and 14. On the other hand, the particle path in the present analysis is determined as part of the solution: It is integrated directly from the stagnation point as just described. Furthermore, the position of the nascent vortex can be taken arbitrarily close to the trailing edge without incurring a numerical problem, as the change in vortex strength Δk ($= k_{N+1}$) for each time step is determined analytically. The following explicit formula for Δk can be readily derived from Eq. (25) by the Kutta condition, which says that the velocity is zero at the trailing edge in the τ plane, and the Kelvin-Helmholtz circulation theorem:

$$\Delta k = \frac{\mathrm{Re}\left[-2U \sin(\alpha - \theta_0) + k - e^{i\theta_0} \sum_{n=1}^{N} k_n \left(\frac{1}{e^{i\theta_0} - \tau_n} + e^{-i\theta_0} - \frac{1}{e^{i\theta_0} - 1/\bar{\tau}_n} \right) \right]}{\mathrm{Re}\left[\left(\frac{1}{e^{i\theta_0} - \tau_{N+1}} - \frac{1}{e^{i\theta_0} - 1/\bar{\tau}_{N+1}} \right) e^{i\theta_0} \right]} \tag{38}$$

where $2\pi k$ is the circulation around the airfoil and is given by

$$k = \sum_{n=1}^{N} k_n - \frac{S}{\pi} [\Psi(t_{N+1}) - \Psi(t_0)]$$

Numerical Examples

The procedure described in the preceding sections is summarized in Fig. 2. It should be noted that the velocity (or pressure) distribution on the surface need not be computed at every time step. A few sample calculations are made to verify the procedure. A symmetric Kármán-Trefftz airfoil is chosen for this purpose. Its thickness/chord ratio is 0.15 and the trailing-edge angle is 9 deg.

The calculation is performed first for steady flow at an angle of incidence of 9 deg. The airfoil contour is divided into 50 segments of equal angle in the ζ plane when solving the integral equation [Eq. (13)]. The pressure distribution for the upper surface is compared with the exact solution in Table 1; a near perfect (four places) agreement is observed. Although this particular airfoil can be transformed onto a circle analytically, the comparison is still legitimate as we do not use the exact node (N in Fig. 1) that would give a circle in the ζ plane. In view of the relatively coarse distribution of integration nodes, the high accuracy obtained here is remarkable; it is mainly attributed to the most accurate quadrature formula for a cyclic integrand.

For unsteady-flow calculations, 180 points around the airfoil are used for accurate aerodynamic-force integration. Considering the fact that the method is highly accurate even with only 50 points, the use of this many points may appear unnecessary. However, since it introduces a relatively small increase in computing time while giving more accurate aerodynamic forces, no attempt was made to find the optimal number of points for the calculation.

The first of the two unsteady motions considered in this paper is the airfoil traveling at a constant speed while executing a sinusoidal heaving motion. The vertical position as a function of time is given by

$$y(t) = 0.018 \sin(\sigma t)$$

as is done in Refs. 1 and 3. The results for $\sigma = 4.3$ are obtained for two different dimensionless time steps, namely, 0.02 and 0.04.

Figure 3 shows the positions of the shed vortices. Each point represents a vortex core that has been shed at an earlier time. The trajectory of the wake is in good qualitative agreement with earlier results for varying geometries.[1-3] The clustering of the trailing vortices is clearly visible in the figure. The phenomenon is much more pronounced as the frequency of the heaving motion becomes higher, as shown in Fig. 4 ($\sigma = 17$, $\Delta t = 0.005$).

The aerodynamic coefficients of lift C_L, drag C_D, and moment about the nose C_M, are shown in Figs. 5 and 6. These quantities have been evaluated by integrating the pressure [Eq. (23)] over the surface. The circulation around the airfoil, $2\pi k$, is also shown in Fig. 6. As seen in Figs. 3 and 5, the results for two different time steps are in good agreement with each other and, thus, confirm that convergence has been attained. Overall, the results compare favorably with those of Kim and Mook.[3] The drag is small but negative, implying a small forward thrust. The lift is completely out of phase with the circulation and leads the vertical velocity by approximately $\pi/2$. The phase shift is in agreement with that indicated in Kármán and Sears[15]; it is because of the high reduced frequency of the motion, which makes the apparent-mass effect dominant. The drag becomes a minimum (maximum in magnitude) when the airfoil passes the mean position of oscillation and is of larger magnitude when the foil is moving away from the mean position than when approaching the mean position. Here, it needs to be pointed out that the curves in Fig. 6 for circulation and drag vs airfoil position differ from those of a similar figure in Ref. 3 (Fig. 10). There, the circulation is out of phase relative to the present result while the drag curve appears to be upside down. These trends appear to be inconsistent with results shown in Ref. 3 (Fig. 9), where forces, plotted against the phase angle, agree with the present results shown in Figs. 5 and 6.

A calculation was also made, with a time step of 0.01, for the same airfoil moved impulsively from rest to a speed U_∞ at

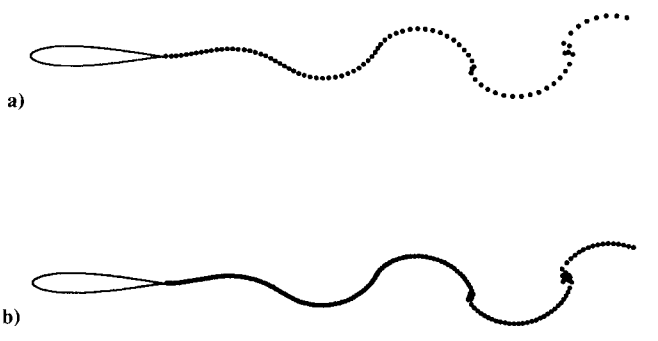

Fig. 3 Wake trajectory behind the sinusoidally heaving airfoil for $\sigma = 4.3$: a) $\Delta t = 0.04$; and b) $\Delta t = 0.02$.

Fig. 4 Wake trajectory behind the sinusoidally heaving airfoil for $\sigma = 17$, $\Delta t = 0.005$.

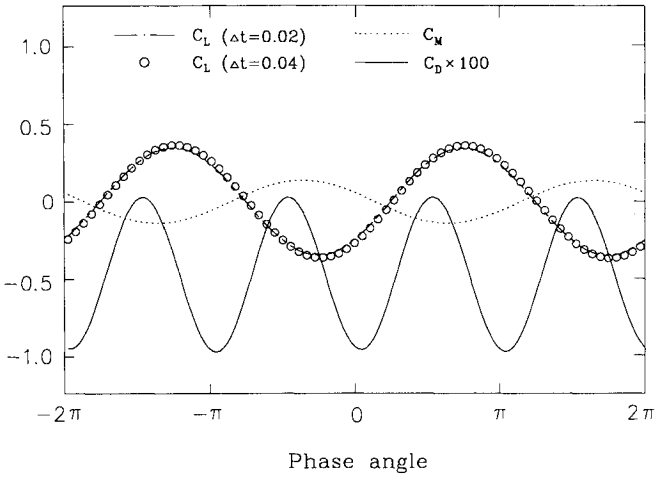

Fig. 5 Aerodynamic forces vs phase angle for the sinusoidally heaving airfoil.

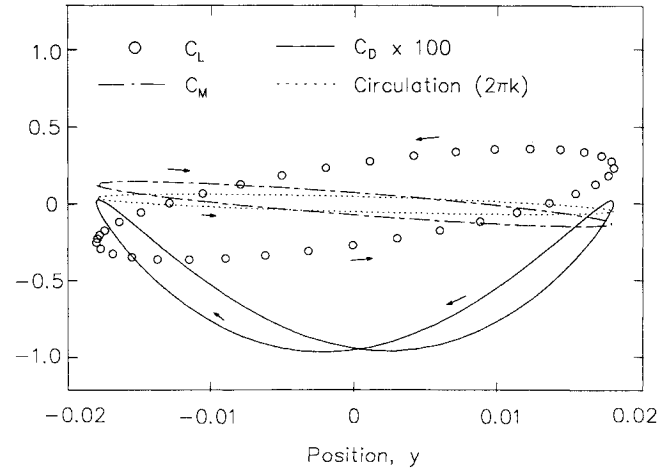

Fig. 6 Aerodynamic forces vs position for the sinusoidally heaving airfoil.

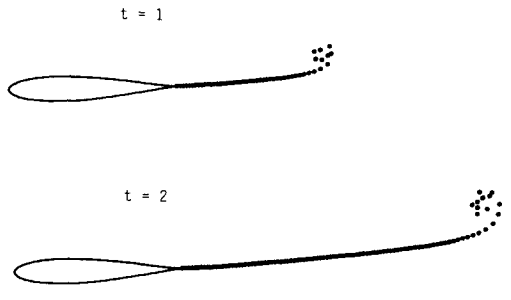

Fig. 7 Wake trajectories for the impulsively started airfoil.

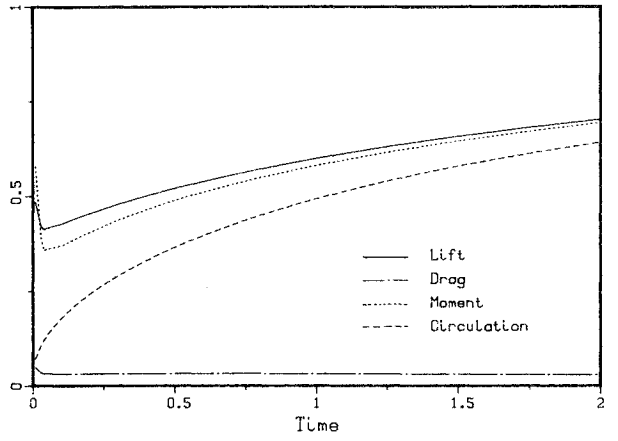

Fig. 8 Aerodynamic forces vs time for the impulsively started airfoil.

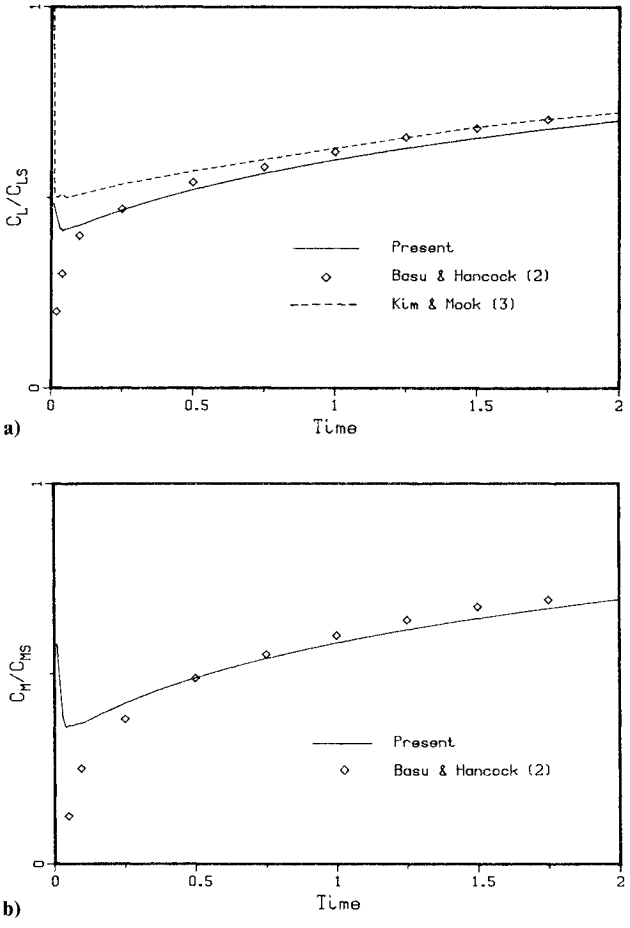

Fig. 9 Comparison of aerodynamic forces with earlier results: a) lift; and b) moment.

a constant 9 deg incidence. The positions of vortex cores, shown in Fig. 7 at two instants, depict the development of vortex rollup very well. The spiral shape of the wake is well captured in the present calculation. Figure 8 shows the lift, drag, moment, and circulation. These have been normalized in terms of their steady-state counterparts except for the drag, which is normalized by the lift. The initial drops in the aerodynamic forces are in qualitative agreement with the results of Kim and Mook[3] and also with those of Graham,[16] who discussed the initial singular behavior in great detail in his analytical work. The lift and moment are compared with earlier results in Fig. 9. The data compared in the figure have been taken graphically from Refs. 2 and 3 and, therefore, are subject to some uncertainty. Again a close agreement between these results is observed. The initial behavior of the starting flow, whether it is finite or singular, is still the subject of controversy[16,17] and it is perhaps beyond the scope of this paper to resolve it. However, in an effort to assess the accuracy of the present scheme, especially at this early stage, an additional calculation has been performed for a thin (3% thick) Joukowski airfoil at a small incidence (1 deg). This is to mimic the classical flat-plate problem of Wagner, and the results are compared in Fig. 10. Both lift and circulation agree well with those in Ref. 18 and this confirms the accuracy of the present nascent vortex model [Eq. (38)]. The lift still exhibits an initial decrease, but to a much lesser extent. Whether it will

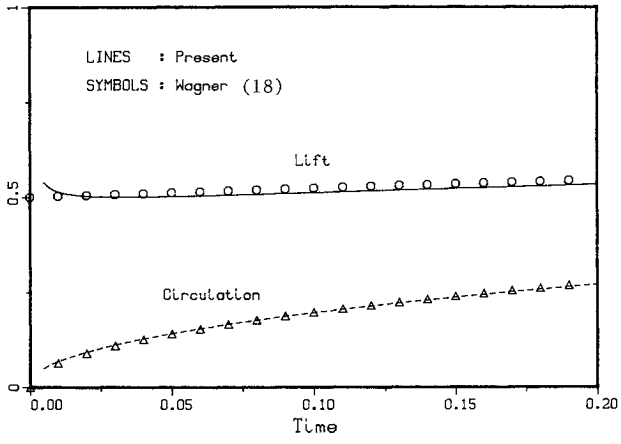

Fig. 10 Initial development of lift and circulation: lines, present (3%-thick Joukowski airfoil); symbols, Wagner (flat plate).

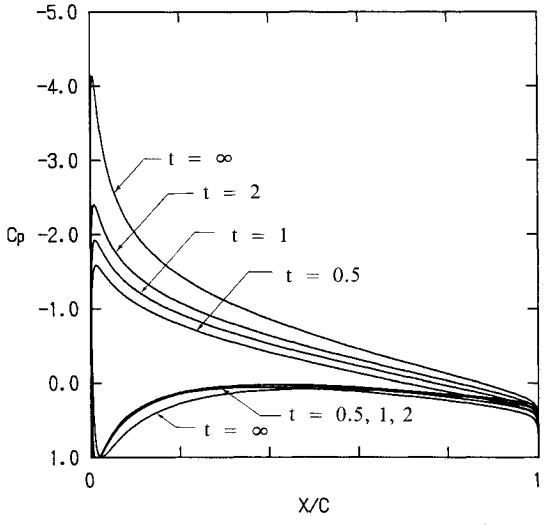

Fig. 11 Pressure distributions for the impulsively started airfoil at various instants.

disappear in the flat-plate limit, as in the Wagner problem, however, is not clear and, therefore, whether the phenomenon is real or numerical due to the discrete vortex model cannot be decided at this stage.

Figure 11 shows the development of the surface pressure distribution with time. It is seen that the pressure on upper and lower surfaces near the trailing edge appear to merge together at all times. This implies that the present Kutta condition is compatible with the condition that the loading be zero at the trailing edge. A note of caution is in order, however. Although the loading seems to be zero for this case, it does not appear to be a good condition to use as a Kutta condition with a discrete-vortex model. This is because the zero-loading condition can be achieved only with a continuous vortex-sheet model where a velocity jump across the sheet occurs.

Finally, to verify the present Kutta condition and its implementation described in the preceding section, additional calculations were made for the purpose of examining the direction of the vortex-core path near the trailing edge. Existing models assume the prevailing direction to be tangent to the body surface. These perform well, in general, except that they fail to recover the steady-state streamlines when the strength of the nascent vortex becomes small.

To visualize the wake line in relation to the surface tangent at the trailing edge more clearly, a Kármán-Trefftz airfoil with a large trailing-edge angle (30 deg) is selected. The angle of incidence is 10 deg and the motion is started impulsively. Figure 12 shows the positions of the cores at four different

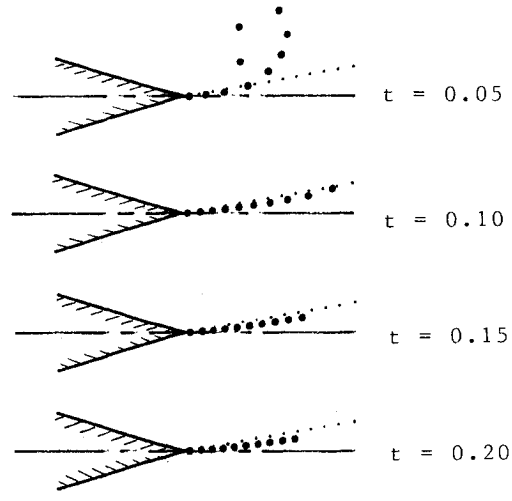

Fig. 12 Vortex trajectories near the trailing edge at various instants for an impulsively started airfoil with a large trailing-edge angle.

instants: $t = 0.05$, 0.1, 0.15, and 0.2. Here, the airfoil portion of the figures represents 3% of the chord length and the dotted line indicates the freestream direction. It is to be noted that the strengths of vortices are greater for small time, gradually decrease with time, and eventually become zero as the steady state is reached. At $t = 0.05$, where the strength is relatively large, the direction of motion of the vortex core is close to the tangent of the lower surface of the airfoil and, thus, is in agreement with the Giesing-Maskell model. However, as time passes, it is seen that its direction is changing toward the direction of the angle bisector, which is the steady-state limit, before it follows the freestream direction a short distance downstream. The ability of the unsteady Kutta condition to recover the steady-state streamlines near the trailing edge is a clear improvement over previous treatment. The fact that it is done automatically can simplify the coding also.

The main advantage of this method is that, once the geometry is transformed, the only remaining portion of the computation is to follow the trailing vorticies. This yields a significant saving in computation time, especially when a large number of points is used or a small time step is taken. Also, since the potential is given analytically, the increment of circulation at each time step can be determined more accurately.

Conclusions

It is shown that the unsteady motion of a two-dimensional airfoil of arbitrary shape can be analyzed using a conformal-mapping technique. The mapping is carried out in an accurate manner by making the integrand of the Gershgorin integral equation cyclic. The procedure should be more efficient than existing panel methods as the integral equation needs to be solved only once to transform the geometry. The Kutta condition applied here, which is applicable to both steady and unsteady flows, is straightforward, robust, and gives the change in circulation very accurately.

Appendix A: Relations Between Bipolar and Polar Coordinate Systems

In terms of the bipolar coordinate systems in the z and ζ planes of Fig. 1,

$$z - \epsilon = R_1 e^{i\psi_1}, \qquad \zeta - l = R_2 e^{i\psi_2} \tag{A1}$$

$$\zeta + 1 = r_1 e^{i\phi_1}, \qquad \zeta - 1 = r_2 e^{i\phi_2}$$

Equations (A1) yield

$$R_2/R_1 = (r_2/r_1)^p, \qquad \psi_2 - \psi_1 = p(\phi_2 - \phi_1) \tag{A2}$$

We wish to obtain relations with the polar coordinates (r,ϕ) in the ζ plane relative to the origin at C. The cosine law, applied to the triangles NCP, CPT, and NPT gives

$$r^2+1+2r\cos\phi=r_1^2$$

$$r^2+1-2r\cos\phi=r_2^2 \tag{A3}$$

$$r_1^2+r_2^2-2r_1r_2\cos\omega=4, \qquad \omega=\phi_2-\phi_1 \tag{A4}$$

Then from Eq. (A3), we obtain

$$\xi=r\cos\phi=\tfrac{1}{4}(r_1^2-r_2^2) \tag{A5}$$

$$r=[\tfrac{1}{2}(r_1^2+r_2^2)-1]^{1/2} \tag{A6}$$

Also, from Eq. (A4), we obtain

$$r_1=2/d, \qquad r_2=2\lambda/d \tag{A7}$$

where

$$\lambda=r_2/r_1 \quad \text{and} \quad d=\sqrt{\lambda^2-2\lambda\cos\omega+1}$$

Next, the law of sines, applied to the same triangles, gives

$$\frac{\sin\phi_2}{r_1}=\frac{\sin\phi_1}{r_2}=\frac{1}{2}\sin\omega \tag{A8}$$

and

$$r\sin\phi=r_1\sin\phi_1=r_2\sin\phi_2 \tag{A9}$$

Eliminating $\sin\phi_1$, we obtain

$$r\sin\phi=\frac{1}{2}r_1r_2\sin\omega \tag{A10}$$

Substituting the relations of Eq. (A7) into Eqs. (A5) and (A10) now yields the following expressions for the rectangular (ξ,η) and polar (r,ϕ) coordinates in the ζ plane, in terms of the bipolar coordinates (λ,ω)

$$\xi=\frac{1-\lambda^2}{d^2}, \qquad \eta=\frac{2\lambda}{d^2}\sin\omega \tag{A11}$$

and

$$r=\frac{1}{d}\sqrt{\lambda^2+2\lambda\cos\omega+1}, \qquad \phi=\tan^{-1}\frac{2\lambda\sin\omega}{1-\lambda^2} \tag{A12}$$

where r_1 and r_2 already have been expressed in terms of (λ, ω) in Eq. (A8). Then ϕ_1 and ϕ_2 can be obtained either from Eq. (A9) or from

$$\phi_1=\tan^{-1}\frac{\eta}{\xi+1}, \qquad \phi_2=\tan^{-1}\frac{\eta}{\xi-1} \tag{A13}$$

The latter are preferable since there would be a loss of accuracy in calculating ϕ_1 or ϕ_2 from Eqs. (A9) when either angle is near $\pi/2$.

Inversely, when (ξ,η) or (r,ϕ) are given, the values of r_1, r_2, ϕ_1, ϕ_2, λ, and ω are given by

$$r_1=[(\xi+1)^2+\eta^2]^{1/2}=[r^2+2r\cos\phi+1]^{1/2}$$

$$r_2=[(\xi-1)^2+\eta^2]^{1/2}=[r^2-2r\cos\phi+1]^{1/2} \tag{A14}$$

and ϕ_1 and ϕ_2 by Eq. (A13). Then ω can be obtained from

$$\omega=\phi_2-\phi_1=\tan^{-1}\frac{2\eta}{\xi^2+\eta^2-1}=\tan^{-1}\frac{2r\sin\phi}{r^2-1} \tag{A15}$$

The ω can also be calculated from Eqs. (A4) or (A8), but with some loss of accuracy from Eqs. (A4) when θ is small, and from Eqs. (A8) when ω is near $\pi/2$.

Appendix B: Kelvin-Helmholtz Circulation Theorem in a Noninertial Coordinate System

In an inertial coordinate system, the position vector of a point on the moving closed curve will be expressed in the parametric form $\boldsymbol{R}=\boldsymbol{R}(s,t)$, where s is constant for each material fluid particle of the curve and is independent of the time t. Let $\boldsymbol{R}_0(t)$ be the position vector of the origin of a noninertial coordinate system and $\boldsymbol{R}_r$ be the position vector of a point relative to that coordinate system. Let $\boldsymbol{V}_0(t)$ denote the velocity of the point $\boldsymbol{R}_0$ and $\Psi(t)$ the angular velocity of the noninertial coordinate system. Then we have

$$\boldsymbol{R}=\boldsymbol{R}_0+\boldsymbol{R}_r(s), \qquad \boldsymbol{V}=\boldsymbol{V}_0+\boldsymbol{V}_r+\Psi\times\boldsymbol{R}_r \tag{B1}$$

Taking the curve C to be the profile of the airfoil, the circulation Γ about the airfoil section in the inertial system is

$$\Gamma=\oint \boldsymbol{V}\cdot\frac{\partial\boldsymbol{R}}{\partial s}\,ds$$

or

$$\Gamma=\oint(\boldsymbol{V}_0+\boldsymbol{V}_r+\Psi\times\boldsymbol{R}_r)\cdot\frac{\partial\boldsymbol{R}_r}{\partial s}\,ds \tag{B2}$$

But

$$\oint \boldsymbol{V}_0\cdot\frac{\partial\boldsymbol{R}_r}{\partial s}\,ds=\boldsymbol{V}_0\cdot\oint\frac{\partial\boldsymbol{R}_r}{\partial s}\,ds=0 \tag{B3}$$

$$\oint \Psi\times\boldsymbol{R}_r\cdot\frac{\partial\boldsymbol{R}_r}{\partial s}\,ds=\Psi\cdot\oint\boldsymbol{R}_r\times\frac{\partial\boldsymbol{R}_r}{\partial s}\,ds$$

$$=\Psi\oint\left(x\frac{\partial y}{\partial s}-y\frac{\partial x}{\partial s}\right)ds \tag{B4}$$

for the two-dimensional case of the present paper, with $\Psi=\hat{k}\Psi$ and $\boldsymbol{R}_r=\hat{i}x+\hat{j}y$, and $\hat{i}$, $\hat{j}$, $\hat{k}$ denoting unit vectors in the x, y, z directions of the moving coordinate system. Also we have $\oint y\,dx=-S$, and $\oint x\,dy=S$, where S is the area bounded by the curve C, so that the right-most member of Eqs. (B4) becomes $2S\Psi(t)$. Hence, substituting these results into Eq. (B2), we obtain the relation between the circulations in the two coordinate systems,

$$\Gamma=\Gamma_r+2S\Psi(t) \tag{B5}$$

where $\Gamma_r=\oint\boldsymbol{V}_r\cdot d\boldsymbol{R}_r$ is the relative circulation. If we replace the space occupied by the airfoil by fluid at rest relative to the airfoil, then, since the vorticity of a fluid element is twice its angular velocity, the additional term $2S\Psi$ is seen to be simply the additional circulation due to this entrained vorticity. If $\Psi=0$, then $\Gamma_r=\Gamma$, i.e., no correction is needed.

Similarly, the circulation about a point vortex outside the airfoil can also be related by Eq. (B5). Since the closed path around the vortex can be taken arbitrarily small, the circulations in the two coordinate systems are equal. Finally, if we apply the Kelvin theorem, the relative circulation about the airfoil can be expressed as

$$\Gamma_r=-\Gamma_v-2S\Psi(t)+\text{ const} \tag{B6}$$

where Γ_v is the relative circulation about the shed vortices.

References

[1]Giesing, J. P., "Nonlinear Two-Dimensional Unsteady Potential Flow with Lift," *Journal of Aircraft*, Vol. 5, No. 2, 1968, pp. 135–143.

[2]Basu, B. C., and Hancock, G. J., "The Unsteady Motion of a Two-Dimensional Airfoil in Incompressible Inviscid Flow," *Journal of Fluid Mechanics,* Vol. 87, Part 1, 1978, pp. 159–178.

[3]Kim, M. J., and Mook, D. T., "Application of Continuous Vorticity Panels to General Unsteady Incompressible Two-Dimensional Lifting Flows," *Journal of Aircraft,* Vol. 23, No. 6, 1986, pp. 464–471.

[4]Stern, F., "Comparison of Computational and Experimental Unsteady Cavitation on a Pitching Foil," *Journal of Fluids Engineering* (to be published).

[5]Ardonceau, P. L., "Computation of the Potential Flow over Airfoils with Cusped or Thin Trailing Edges," *AIAA Journal*, Vol. 24, No. 8, 1986, pp. 1375–1377.

[6]Birkhoff, G., Young, D. M., and Zarantonello, E. H., "Numerical Methods in Conformal Mapping," *Proceedings of Symposia in Applied Mathematics, Fluid Dynamics,* Vol. 4, McGraw-Hill, New York, 1953, pp. 117–140.

[7]Halsey, N. D., "Potential Flow Analysis of Multielement Airfoils Using Conformal Mapping," *AIAA Journal*, Vol. 17, No. 12, 1979, pp. 1281–1288.

[8]Poling, D. R., Wilder, M. C., and Telionis, D. P., "Two-Dimensional Interaction of Vortices with a Blade," AIAA Paper 88-0044, Jan. 1988.

[9]Theodorsen, T., "Theory of Wing Sections of Arbitrary Shape," NACA TR 411, 1931.

[10]Landweber, L., and Macagno, M., "Accurate Parametric Representation of Ship Sections by Conformal Mapping," *Proceedings of the First International Conference on Numerical Ship Hydrodynamics,* Oct. 1975, pp. 665–682.

[11]Atkinson, K. E., *An Introduction to Numerical Analysis,* 2nd ed., Wiley, 1988, pp. 285–289.

[12]Milne-Thomson, L. M., *Theoretical Hyrodynamics,* 5th ed., Macmillan, London, 1968, pp. 371–373.

[13]Giesing, J. P., "Vorticity and Kutta Condition for Unsteady Multienergy Flows," *Journal of Applied Mechanics,* Sept. 1969, pp. 608–613.

[14]Poling, D. R., and Telionis, D. P., "The Response of Airfoils to Periodic Disturbances—The Unsteady Kutta Condition," *AIAA Journal,* Vol. 24, No. 2, 1986, pp. 193–199.

[15]von Kármán, T., and Sears, W. R., "Airfoil Theory for Non-Uniform Motion," *Journal of Aeronautical Sciences,* Vol. 5, Aug. 1938, pp. 379–390.

[16]Graham, J. M. R., "The Lift on an Aerofoil in Starting Flow," *Journal of Fluid Mechanics,* Vol. 133, 1983, pp. 413–425.

[17]Chow, C.-Y., and Huang, M.-K., "The Initial Lift and Drag of an Impulsively Started Airfoil of Finite Thickness," *Journal of Fluid Mechanics,* Vol. 118, 1982, pp. 393–409.

[18]Sears, W. R., "Operational Methods in the Theory of Airfoils in Non-Uniform Motion," *Journal of the Franklin Institute,* Vol. 230, No. 1, July 1940, pp. 95–111.